

## Article

# Synthesis and Characterisation of 4D-Printed NVCL-co-DEGDA Resin Using Stereolithography 3D Printing

Elaine Halligan <sup>1,\*</sup>, Billy Shu Hieng Tie <sup>1</sup>, Declan Mary Colbert <sup>1</sup>, Mohamad Alsaadi <sup>1,2</sup>, Shuo Zhuo <sup>1</sup>,  
Gavin Keane <sup>3</sup> and Luke M. Geever <sup>4,\*</sup>

<sup>1</sup> Polymer, Recycling, Industrial, Sustainability and Manufacturing (PRISM) Center, Technological University of the Shannon, Midlands Midwest, Dublin Road, N37 HD68 Athlone, Co. Westmeath, Ireland; a00248520@student.tus.ie (B.S.H.T.); declan.colbert@tus.ie (D.M.C.); mohamad.alsaadi@tus.ie (M.A.); a00238048@student.tus.ie (S.Z.)

<sup>2</sup> CONFIRM Centre for Smart Manufacturing, University of Limerick, V94 T9PX Limerick, Co. Limerick, Ireland

<sup>3</sup> Centre for Industrial Service and Design, Technological University of the Shannon, Midlands Midwest, Dublin Road, N37 HD68 Athlone, Co. Westmeath, Ireland; gkeane@tus.ie

<sup>4</sup> Applied Polymer Technologies Gateway, Material Research Institute, Technological University of the Shannon, Midlands Midwest, Dublin Road, N37 HD68 Athlone, Co. Westmeath, Ireland

\* Correspondence: a00218425@student.tus.ie (E.H.); lgeever@tus.ie (L.M.G.)

**Abstract:** The design and manufacturing of objects in various industries have been fundamentally altered by the introduction of D-dimensional (3D) and four-dimensional (4D) printing technologies. Four-dimensional printing, a relatively new technique, has emerged as a result of the ongoing development and advancements in 3D printing. In this study, a stimulus-responsive material, N-Vinylcaprolactam-co-DEGDA (NVCL-co-DEGDA) resin, was synthesised by Stereolithography (SLA) 3D printing technique. The N-Vinylcaprolactam-co-DEGDA resins were initiated by the Diphenyl (2,4,6-trimethylbenzoyl) phosphine oxide (TPO) photoinitiator. A range of Di(ethylene glycol) diacrylate (DEGDA) concentrations in the NVCL-co-DEGDA resin was explored, ranging from 5 wt% to 40 wt%. The structural properties of the 3D printed objects were investigated by conducting Attenuated Total Reflectance–Fourier Transform Infrared Spectroscopy (ATR-FTIR). Additionally, the 3D printed samples underwent further characterisation through differential scanning calorimetry (DSC) and swelling analysis. The results revealed an inverse relationship between DEGDA concentration and  $T_g$  values, indicating that higher concentrations of DEGDA resulted in lower  $T_g$  values. Additionally, the pulsatile swelling studies demonstrated that increasing DEGDA concentration prolonged the time required to reach the maximum swelling ratio. These findings highlight the influence of DEGDA concentration on both the thermal properties and swelling behaviour of 3D printed samples.

**Keywords:** 3D printing; 4D printing; shape memory polymers; N-vinylcaprolactam; stereolithography



**Citation:** Halligan, E.; Tie, B.S.H.; Colbert, D.M.; Alsaadi, M.; Zhuo, S.; Keane, G.; Geever, L.M. Synthesis and Characterisation of 4D-Printed NVCL-co-DEGDA Resin Using Stereolithography 3D Printing. *Macromol* **2024**, *4*, 150–164. <https://doi.org/10.3390/macromol4010008>

Academic Editor: Andrea Sorrentino

Received: 5 September 2023

Revised: 27 February 2024

Accepted: 8 March 2024

Published: 19 March 2024



**Copyright:** © 2024 by the authors. Licensee MDPI, Basel, Switzerland. This article is an open access article distributed under the terms and conditions of the Creative Commons Attribution (CC BY) license (<https://creativecommons.org/licenses/by/4.0/>).

## 1. Introduction

3D printing, also known as additive manufacturing, is a groundbreaking technology enabling the transformation of digital designs into simple and complex 3D objects. The technology builds an object layer by layer that uses many materials including polymers, metals, ceramics, composites, or smart materials. 3D printing has revolutionised various fields, including the aerospace industry [1], automotive industry [2], food industry, and especially within the healthcare and medical industry, with advancements in prosthetics, pharmaceutical research, implants, and patient-specific treatments [3–5].

The principles and fundamentals of 3D printing provided the groundwork for the emergence of 4D printing. The technique prints simple or complex objects layer by layer using computer-aided design (CAD) software [6]. 4D printing emerged from the development of 3D printing, using the same technique as 3D printing with an extra dimension of

time. In simple terms, 4D printing is 3D printing with smart materials to create an object in which the shape of the object will transform over time when exposed to a stimulus [7]. The stimuli used for the transformation can be pH, water, electric current, light, etc. The fourth dimension refers to the ability of the object to change shape autonomously. 4D printing can be achieved by either one of the following printing processes once the material used for printing is compatible with the printer: stereolithography (SLA), selective laser sintering (SLS), fused deposition modelling (FDM), jet 3D printing (3DP), selective laser melting (SLM), electron beam melting (EBM), or direct ink writing (DIW) [8]. SLA uses a liquid photopolymer resin to create the 3D object. SLA 3D printing uses a UV light source that cures the resin, thereby solidifying the resin layer by layer to create the desired object. SLA 3D printing enables rapid prototyping and produces objects with excellent surface finish and dimensional accuracy [9]. SLA printing can use a wide range of materials with resins that can have different mechanical properties, flexibility, and transparency. In this work, a Form 2 SLA 3D printer was used to fabricate the objects for testing. The Form 2 SLA 3D printer, developed by Formlabs, produces high-resolution 3D prints [10]. The mechanism of the Form 2 SLA uses a UV laser that falls onto the liquid resin present in the resin tank. The Form 2 SLA print is constructed in a stepwise manner: first, the build platform is lowered into the resin tank. Then, galvanometers guide a UV laser through a transparent window located at the bottom of the resin tank, causing the material to solidify. This process is repeated for each successive layer of the print.

Smart materials, also known as programmable materials, are a class of materials that respond and adapt to changes in their environment making them an ideal material for successful 4D printing [11]. Smart materials can be defined as materials which exhibit dynamic properties and respond to external stimuli by changing their physical or chemical characteristics [12]. They can sense, react, and adapt to their surroundings in a controlled and predictable manner. Smart materials can be classified into several categories based on the type of stimulus they respond to, such as temperature, light, pressure, electric fields, magnetic fields, pH, or moisture [13]. The type of smart material used will determine the self-transformation of the 4D printed object. Smart materials can change their properties over a period of time when exposed to an external stimulus; these smart materials can show self-assembly, self-healing, self-capability, or shape memory behaviours [14]. Another advantageous aspect of using smart materials is 4D printing with materials that can generate colour change by exposing the material to UV light or visible light [7].

The adaptive nature of 4D printed structures opens up a wide range of applications across various industries, including the medical field, where significant advancements can be made. One notable application is the production of patient-specific implants and prosthetics [15]. Additionally, 4D printing has the potential to make significant contributions to the field of tissue engineering by allowing the creation of functional biological constructs intended for applications in regenerative medicine [16]. Other 4D potential applications include the self-assembly of furniture [7], the use of adaptive textiles that can adjust their shape or colour based on environmental conditions [17,18], and the use of responsive materials to enable the self-repairing of structures, such as self-healing pipes [7].

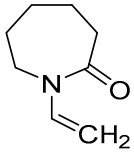
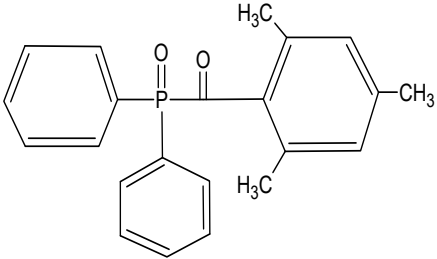
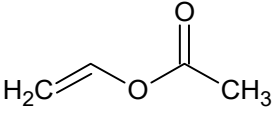
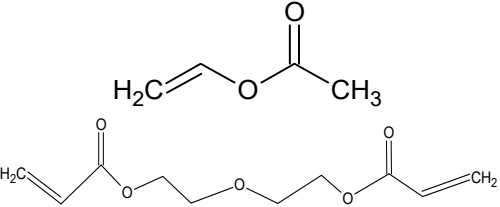
In this work, DEGDA is used, and when combined with a monomer, N-vinylcaprolactam (NVCL), a shape memory polymer is formed, which responds to a temperature-based stimulus. Poly(N-vinylcaprolactam) (PNVCL), a thermoresponsive polymer, exhibits a unique property known as the lower critical solution temperature (LCST), allowing for a reversible phase transition in response to changes in temperature. Thereby making PNVCL an interesting material for 4D printing. PNVCL is considered biocompatible, making it suitable for biomedical applications [19]. One limitation of this combination of materials for 4D printing is that the transformation must occur in water.

## 2. Materials and Methods

### 2.1. Materials

NVCL, acquired from Sigma Aldrich in Co. Dublin, Ireland, is the primary material used, with a molecular weight of 139.19 g/mol. It is stored within a temperature range of 2 to 8 °C. The photoinitiator employed in the process is Diphenyl (2,4,6-trimethylbenzoyl) phosphine oxide (TPO), also acquired from Sigma Aldrich in Co. Dublin, Ireland. The crosslinker employed is DEGDA, with a molecular weight of 214.22 g/mol, sourced from Sigma Aldrich in Co. Dublin, Ireland. The chemical structures of these materials are provided in Table 1.

**Table 1.** The names and chemical structures of the chosen materials.

Material	Chemical Structures
N-vinylcaprolatam (NVCL)	
Diphenyl(2,4,6-trimethylbenzoyl) phosphine oxide (TPO)	
Vinylacetate (VAc)	
Di(ethylene glycol) diacrylate (DEGDA)	

### 2.2. Preparation of NVCL-co-DEGDA Resin

An amorphous resin polymer comprises three important parts: the monomer, the crosslinker, and the photoinitiator. In this study, the monomer used was NVCL, while the crosslinker was DEGDA. A comonomer, VAc, was employed for one of the liquid resins. To maintain sample uniformity, the photoinitiator TPO was introduced into the mixtures at a concentration of 2 wt%. TPO functions as a curing agent during the photoreaction process. The Form 2 SLA 3D printer (manufactured by Formlab in Berlin, Germany) was employed for printing all the samples.

The blends were formulated by precisely measuring and combining specific quantities of NVCL, TPO, DEGDA, and VAc. Initially, the photoinitiator was dissolved in 3 mL of Methanol prior to the addition of the mixtures. This step was completed to ensure that the photoinitiator was fully dissolved before adding the resin. DEGDA was added to the glass beaker, consisting of the NVCL monomer, by a drop-wise addition. Each batch was deposited into a 500 mL glass beaker and underwent thorough mixing at 300 rpm with the aid of a magnetic stir bar for a duration of 1 h. Then, the mixtures were poured into the resin tank of the SLA 3D printer. The selected STL file was uploaded onto the printer and after successful printing, the samples were subjected to a 20 min UV chamber drying process prior to use. The formulations of NVCL-co-DEGDA resins for the samples are presented in Table 2.

**Table 2.** ID Code and compositions of resin subsequent to 3D printing.

CODE	Formulation	Photoinitiator	Monomer	Crosslinker	Comonomer
		TPO (wt%)	NVCL (wt%)	DEGDA (wt%)	VAc (wt%)
V1	P(NVCL95-DEGDA5)	2	95	5	--
V2	P(NVCL90-DEGDA10)	2	90	10	--
V3	P(NVCL80-DEGDA20)	2	80	20	--
V4	P(NVCL70-DEGDA30)	2	70	30	--
V5	P(NVCL60-DEGDA40)	2	60	40	--
V6	P(NVCL70-DEGDA10-VAc20)	2	70	10	20

### 2.3. Attenuated Total Reflectance–Fourier Transform Infrared Spectroscopy

Attenuated Total Reflectance–Fourier Transform Infrared Spectroscopy (ATR-FTIR) analysis was carried out using a Perkin Elmer Spectrum One FT-IR Spectrometer (C-001) manufactured in Waltham, MA, USA. The spectrometer was equipped with a universal ATR sampling accessory. The analysis was conducted at an approximate temperature of 22 °C and covering a spectral range spanning from 4000 to 650 cm<sup>-1</sup>. Throughout the analysis, a consistent and reliable approach was maintained by applying a fixed universal compression load of 75 N, and each sample underwent 4 scans.

### 2.4. Differential Scanning Calorimetry

Differential scanning calorimetry (DSC) was employed to observe the thermal transitions of the 3D prints. To prepare the samples, an appropriate amount, typically ranging from 8 to 12 mg, was accurately weighed using a Sartorius balance (Sartorius, Goettingen, Germany) with a resolution of 0.01 mg. These samples were then placed in hermetically sealed aluminium pans, which were securely crimped prior to testing. The analysis was conducted using a TA Instruments DSC 2920 (New Castle, DE, USA) equipped with a modulated differential scanning calorimeter. Prior to the analysis, the instrument underwent calibration using indium as a standard reference material. The scans were performed at a rate of 10 °C/min, spanning from 20 to 200 °C. To ensure the removal of volatiles from the purging head, a flow of nitrogen gas at a rate of 30 mL/min was employed.

### 2.5. Pulsatile Swelling Studies

Following the 3D printing process, the chemically crosslinked samples underwent a 24 h vacuum drying phase at 50 °C. The initial dry weight of the 3D printed samples was determined with high precision using a Sartorius balance, with a resolution of 1 × 10<sup>-5</sup>, this weight was denoted as  $W_d$ . Once prepared, the samples were placed within rectangular plastic containers containing 350 mL of distilled water with a pH level of 7.1. Subsequently, the samples were tested both at room temperature and at 50 °C. At specific time intervals, the samples were extracted from the rectangular plastic containers, and any excess surface water was eliminated using filter paper. The resulting weight, noted as " $W_t$ ", represented the wet weight of the samples. All experimental samples underwent triplicate testing. The swelling ratio was determined using Equation (1).

$$\text{Swelling Ratio (\%)} = ((W_t - W_d)/W_d) \times 100 \quad (1)$$

where  $W_t$  signifies the weight of the gel at a designated time, whereas  $W_d$  denotes the mass of the polymer when it is completely dry state.

### 2.6. Gel Fraction

The efficiency of hydrogel network formation can be quantitatively evaluated using gel fraction measurement [20]. To measure the gel fraction of all batches, a round disc was used. The 3D printed samples were placed in covered Petri dishes containing 30 mL of distilled water and left at room temperature until they reached a state of equilibrium

swelling. Once equilibrium swelling was achieved, the samples were dried in a vacuum oven at 50 °C and 100 Pa until no further changes in weight were observed. The gel fraction percentage of the samples was then calculated using the following formula:

$$\text{Gel fraction (\%)} = (W_d/W_0) \times 100 \quad (2)$$

where  $W_0$  refers to the initial weight of the dried sample, while  $W_d$  corresponds to the weight of the dried, insoluble fraction of the sample following its extraction with water.

### 2.7. Goniometry

Contact angle goniometry was employed to assess the solid substrate's resistance to liquids. In this procedure, a dynamic sessile droplet of water was deposited onto the surface of the 3D printed samples, and photographs were captured to document the droplet's spread [21]. The samples were positioned on the stage, and the angle measurement was automatically derived from the captured photos. To evaluate the wettability of the 3D printed samples, photographs were taken at two time points: 0 s and 115 s. All experiments were performed in triplicate.

### 2.8. Recrystallisation Test

Prior to 3D printing, 10 g of each sample was prepared and placed into 25 mL glass beakers. This step aimed to investigate the potential occurrence of recrystallisation in the liquid formulations. The test was conducted at room temperature, aiming to assess recrystallisation behaviour. In order to visualise and compare the differences between the resins, photographs of the samples were taken.

## 3. Results

### 3.1. Preparation of NVCL-co-DEGDA Resin

Photopolymerisation is a polymerisation technique in which visible or UV light is employed to create in situ cross-linkages for the polymerisation of a sample [22]. 3D printing offers numerous advantages over traditional polymerisation techniques, such as design flexibility, customisation and personalisation, rapid prototyping, and fabrication of complex structures [23].

The NVCL-co DEGDA resins were printed in the presence of a 2 wt% TPO photoinitiator. When exposed to UV light, TPO undergoes a photochemical reaction called photolysis. During photolysis, TPO absorbs UV photons and undergoes a chemical change, thereby generating free radicals. These free radicals, in turn, initiate the polymerisation of the NVCL monomer. The free radicals generated from the TPO photoinitiator react with the double bonds in NVCL, initiating a chain reaction that leads to the formation of a 3D polymer network. The liquid resin gradually solidifies and hardens, transforming into a solid to cure the object layer by layer. The Form 2 SLA 3D printer uses a wavelength of 405 nm for its laser source [24]. The print quality of the Form 2 SLA printer is exceptional with a layer resolution as low as 25 microns. DEGDA can improve the mechanical strength and stability of a printed object by acting as a crosslinking agent [25]. DEGDA can also be used as a shape-memory component, allowing the 4D printed objects to undergo reversible shape changes when exposed to specific triggers.

A CAD file of the disc samples (thickness of 5 mm and diameter of 40 mm) was uploaded onto the Form 2 SLA 3D printer to print the test samples. The Open Mode feature was used on the Form 2 SLA 3D printer to allow for successful printing with the formulated liquid NVCL-co-DEGDA resin formulations presented in Table 2. Figure 1 illustrates that all the samples underwent successful curing and retained their structural integrity after the printing process. Open Mode allows for using a broad range of materials beyond the ones specifically designed and approved by the printer manufacturer. All disc samples were printed directly onto the build platform with no support generated for the discs. By printing directly onto the build platform, optimal disc samples were obtained, as displayed in Figure 2.

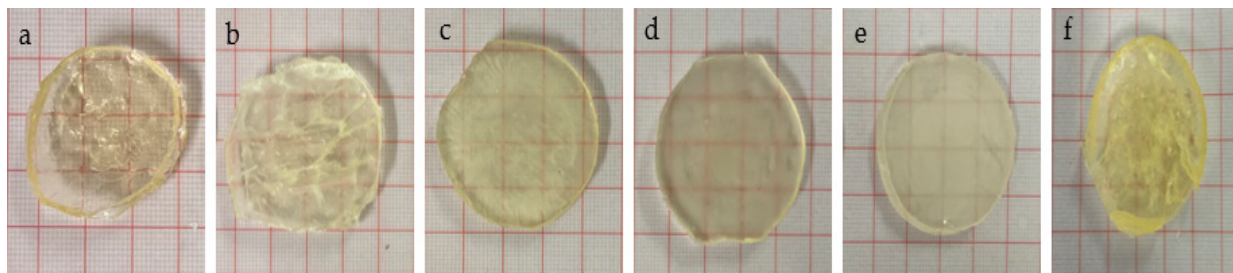


**Figure 1.** 3D printed test samples fabricated with varying proportions of DEGDA/VAc with 2 wt% TPO photoinitiator (a) V1, (b) V2, (c) V3, (d) V4, (e) V5, and (f) V6.

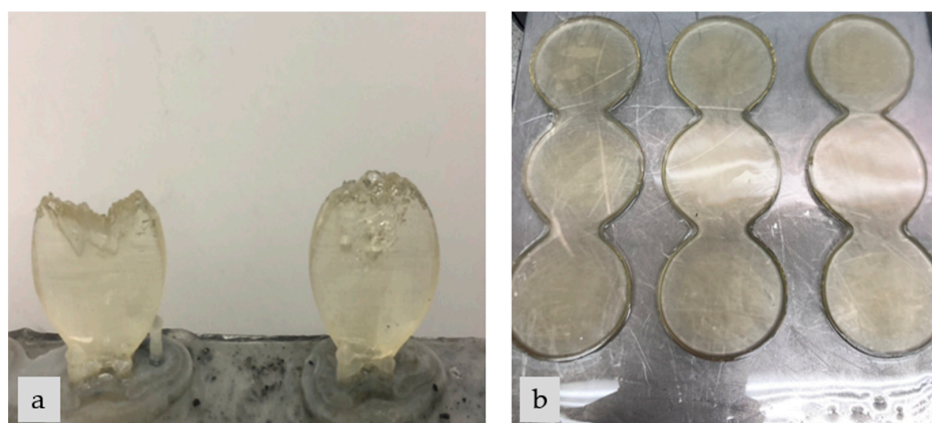


**Figure 2.** 3D printing the test samples (a) with supports and (b) directly onto the build platform.

### 3.2. Recrystallisation Test

Recrystallisation is a process by which a solid material transitions from an amorphous state to a crystalline structure [26]. In the case of NVCL, it is considered an amorphous polymer [27] and will recrystallise due to its molecular structure. Prior to 3D printing, each sample was tested to investigate the potential occurrence of recrystallisation in the liquid formulations. NVCL 100 wt% was tested along with the formulations presented in Table 2. In order to successfully 3D print, the recrystallisation behavior of all formulations had to be visualised. The Form 2 SLA 3D printer used in this study was operated by the Open Mode feature, which allowed the use of third-party resin to be printed. However, in open mode, the printer did not allow for the control of temperature. Figure 3 illustrates the recrystallisation of pure NVCL, with no crosslinker or comonomer present. NVCL 100 wt% showed crystallisation at room temperature within 30 min. The samples formulated with 5 wt% DEGDA, sample V1, and as high as 40 wt% DEGDA, sample V5, showed no signs of recrystallisation at room temperature throughout 8 h. Also, sample V6 showed no signs of recrystallisation at room temperature throughout 8 h.

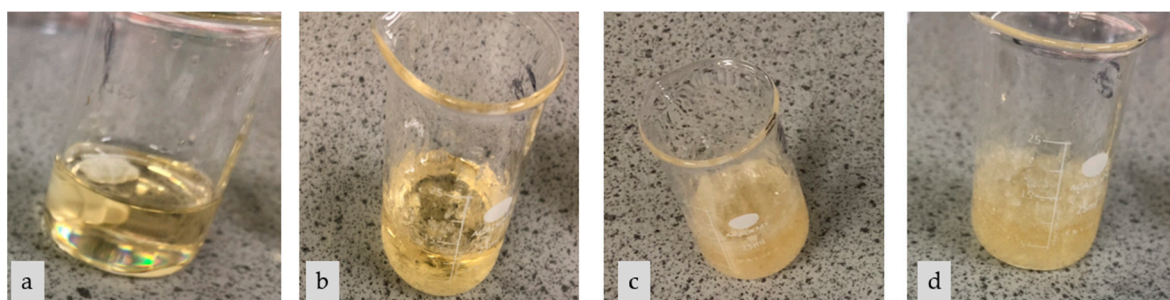


**Figure 3.** The recrystallisation of NVCL 100 wt% (a) 0 min, (b) 10 min, (c) 30 min, and (d) 1 h.

### 3.3. Attenuated Total Reflectance Fourier Transform Infrared Spectroscopy

ATR-FTIR spectroscopy is a powerful analytical technique used to investigate the chemical composition and structure of materials. In this study, ATR-FTIR spectroscopy analysed the chemical structure of monomers as well as the photopolymerised samples. This technique involves exposing a sample to infrared radiation through an ATR crystal, where a portion is absorbed by the material, and another portion passes through it (transmission). Various functional groups and chemical bonds display absorption peaks at distinct wavelengths, enabling the identification of functional groups within a sample. In this study, ATR-FTIR spectroscopy was used to distinguish between the chemical bonds found in VAc, NVCL, DEGDA, and the 3D printed samples (V1, V2, V3, V4, V5, and V6). The resultant IR spectra are displayed in Figures 4 and 5, respectively. The correlation of absorption bands with specific functional groups can be found in Table 3.

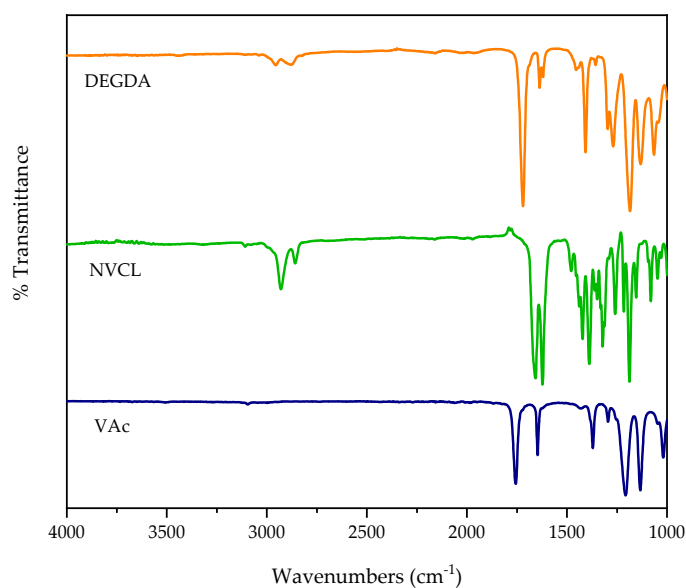


**Figure 4.** FTIR spectra of neat samples DEGDA, NVCL, and VAc (top–bottom).

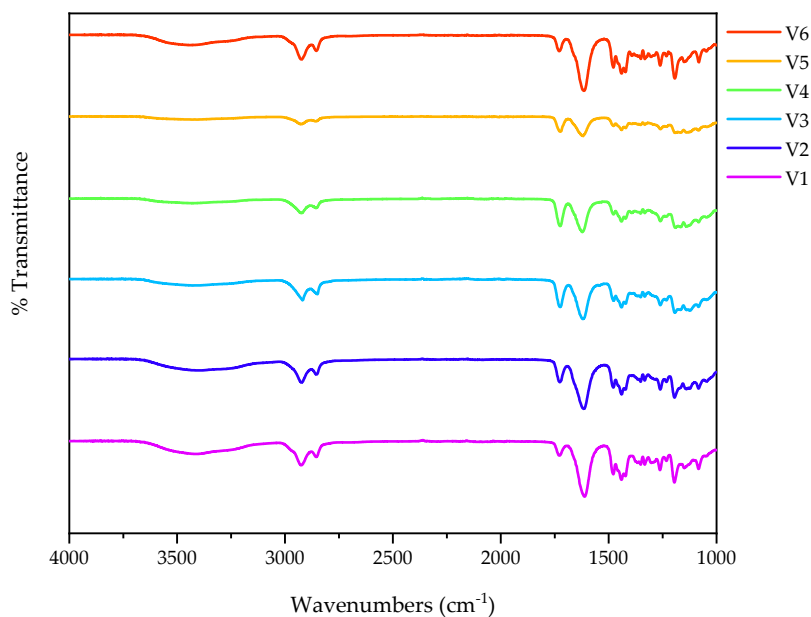


**Figure 5.** FTIR spectra of sample V1, V2, V3, V4, V5, and V6 (bottom–top).

**Table 3.** Identification and explanation of characteristic peaks obtained through ATR-FTIR analysis.

Sample	Wavelength (cm <sup>-1</sup> )	Functional Group
Monomers		
DEGDA	1720	C=O
	1637	C–C
	1185	C–O
VAc	1647	C=O
	1759	C–H
NVCL	2930, 2860	C–H
	1656	C=O
	1620	C=C
	1260	C–N
3D printed Samples		
PNVCL/DEGDA (V1–V5)	1473–1350	C–H
	1710–1730	C=O
PNVCL/DEGDA/VAc (V6)	2854	C–H

The NVCL monomer exhibited a distinctive carbonyl peak at 1656 cm<sup>-1</sup>, signifying the presence of the C=O peak [28]. The peak exhibited at 1620 cm<sup>-1</sup> and 1260 cm<sup>-1</sup> for the NVCL monomer represents the C–C stretching and the C–N stretching, respectively. Finally, the peaks displayed at 2927 cm<sup>-1</sup> and 2862 cm<sup>-1</sup> for the NVCL monomer relate to the aliphatic C–H stretching. Neat DEGDA displayed characteristic absorption bands at 1720 cm<sup>-1</sup>, 1637 cm<sup>-1</sup>, and 1250 cm<sup>-1</sup>. These absorption bands were attributed to the stretching vibrations of the carbonyl (C=O) functional group, the C–C functional group, and the C–O group's stretching vibration. The VAc monomer exhibited a peak at 1647 cm<sup>-1</sup>, 1759 cm<sup>-1</sup>, and 1200 cm<sup>-1</sup>, indicating the stretching vibration of the acetate group's (COO–) C=O and the stretching vibration of the carbonyl group in unconjugated ketones [29].

Differences observed in the IR spectra among samples containing identical constituents typically suggest the occurrence of a chemical reaction. Such variations indicate changes in the chemical structure, which can manifest as shifts in the characteristic peaks observed in the IR spectrum. Post 3D printing, the samples display a new peak, thus indicating that copolymerisation successfully occurred. For the 3D printed samples, there was an appearance of absorption bands from a range of 1473–1350 cm<sup>-1</sup>, representing the varying alkane C–H stretching. The 3D printed samples exhibited a peak from the range of 1710–1730 cm<sup>-1</sup> and 2920–2930 cm<sup>-1</sup>, indicating the presence of the C=O stretching vibrations and the strong alkane C–H compound characteristic of most polymer chains, respectively [30].

### 3.4. Differential Scanning Calorimetry

DSC is a powerful technique used for thermal analysis to study how materials react to variations in temperature, heat capacity, and thermal transformations. This thermal analysis was carried out to investigate the influence of DEGDA and the comonomer VAc on the thermal characteristics of the 3D printed samples.

The glass transition temperature ( $T_g$ ) represents a critical aspect to take into account, as the  $T_g$  can influence the mechanical and thermal properties of a printed material. The diffusion rates of polymers will decrease when below the  $T_g$ . However, the diffusion rates of polymers increase when above the  $T_g$ . The polymer undergoes dissolution when above the  $T_g$ , which, in turn, leads to the creation of a gel layer at the dissolution interface. At the dissolving interface, the chains within the polymer disentangle and diffuse into the surrounding medium. Similarly, when the temperature falls below  $T_g$ , the thickness of the gel layers diminishes, causing a shift in the dissolution mechanism towards an eruption process, during which small polymer blocks are released [31].



PNVCL, a non-crystalline polymer, exhibits a  $T_g$  of 147 °C [27,32,33]. However, it is important to note that the  $T_g$  of PNVCL can be influenced by several factors, including molecular weight, purity, moisture content, and compositional variations [34–36].

The DSC analysis of samples V2 and V5, as displayed in Figure 6, indicated a  $T_g$  of 133.99 °C and 62.63 °C, respectively. An inverse relationship between the  $T_g$  values and the crosslinker concentration was observed. The  $T_g$  values decreased as the amount of DEGDA crosslinker increased in the 3D printed samples. Thus, it was observed that the  $T_g$  of the 3D printed samples was influenced by the concentration of the DEGDA crosslinker. Higher concentrations of DEGDA within the 3D printed samples resulted in lower  $T_g$  values.

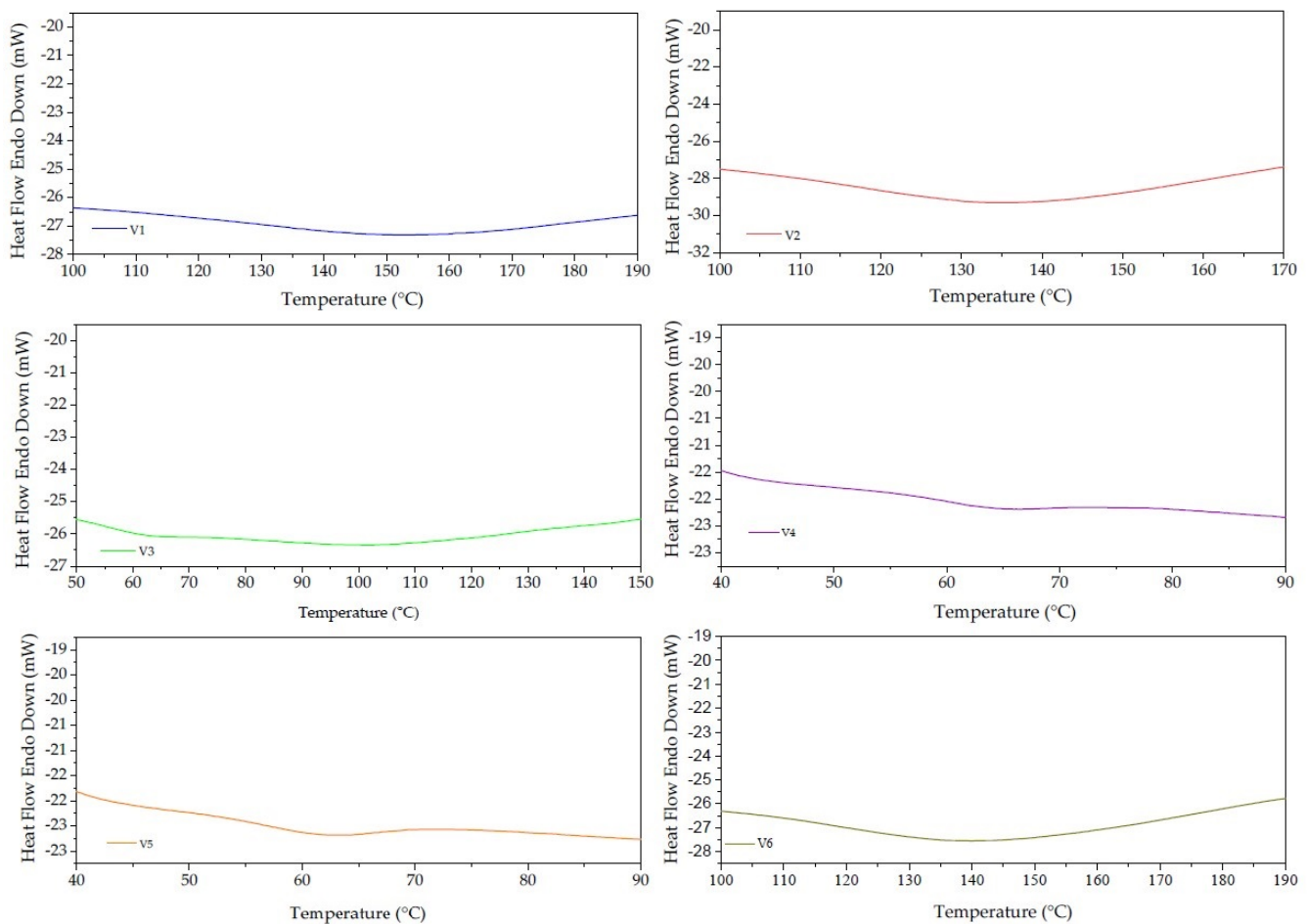


**Figure 6.** DSC thermograph of V1, V2, V3, V4, V5, and V6.

### 3.5. Pulsatile Swelling Studies

To quantify the effect of temperature on the pulsatile swelling properties of the 3D printed samples, swelling analyses were performed at room temperature (22 °C) and at an elevated temperature of 50 °C. The 3D printed samples were chemically crosslinked with DEGDA, ranging from 5 wt% to 40 wt%.

The network structure of the physically crosslinked samples is formed by employing non-covalent interactions, including but not limited to hydrogen bonding, van der Waals forces, and physical entanglements among the polymer chains [37]. Physically crosslinked samples can be reversibly altered, showing poor mechanical properties [34]. Conversely, chemically crosslinked samples undergo a bonding process whereby covalent bonds form between the polymer chains. The formation of covalent bonds leads to the samples' mechanical strength and stability [35]. Materials that undergo chemical crosslinking frequently demonstrate improved thermal and chemical stability as a result of the robust covalent bonds formed between the polymer chains [36].

The extent of crosslinking has an impact on the swelling characteristics of chemically crosslinked samples [38]. The NVCL-co-DEGDA resin was fabricated with five different concentrations of DEGDA: 5 wt%, 10 wt%, 20 wt%, 30 wt%, and 40 wt%. Figure 7 visually presents the results of the swelling analysis conducted on sample V1, which comprises a 5 wt% concentration of DEGDA over 366 h at room temperature and 50 °C.

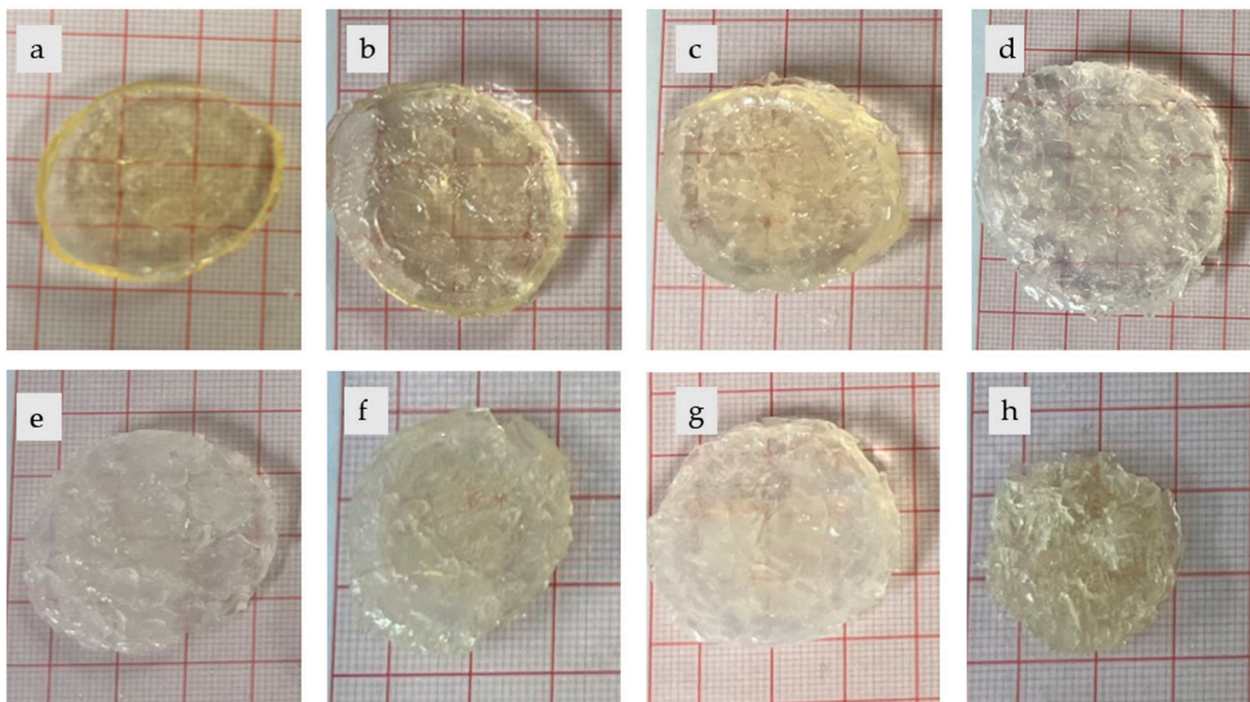


**Figure 7.** The 3D printed sample, V1, underwent a swelling process for a total duration of 504 h. The appearance of the sample was observed at different time intervals: (a) 0 h, (b) 2 h, (c) 3 h, (d) 48 h, (e) 144 h, (f) 168 h, (g) 192 h, and (h) 336 h. Samples (a–e) were observed at room temperature, 22 °C, while samples (f–h) were observed at a temperature of 50 °C.

Figure 8 illustrates the swelling ratio of V2 and V6 at temperatures both below (22 °C) and above (50 °C) the LCST over the course of three cycles. The samples were tested at 22 °C for the first cycle, 1–168 h, then put into the oven, which was set at 50 °C for the period between 168–360 h. Following the samples being exposed to 50 °C, the samples were then placed back to 22 °C for the last cycle (360–504 h). It was noted that a lower concentration of crosslinker in the 3D printed sample led to a faster attainment of the maximum swelling ratio. After 24 h of immersion in distilled water at room temperature, samples V1 and V2, containing 5 wt% and 10 wt% DEGDA, respectively, achieved their maximum swelling ratio. In contrast, samples V4 and V5, with DEGDA concentrations of 30 wt% and 40 wt%, respectively, required 144 h of immersion to reach their maximum swelling ratio. Therefore, it was found that the higher the amount of DEGDA present within the 3D printed sample, the longer it took for the maximum swelling ratio to be reached. These observations align with previous findings in the literature, which also reported that higher crosslink density results in increased resistance to chain extension within hydrogel structures, thereby resulting in a decreased equilibrium swelling degree. Similarly, hydrogels possessing a reduced crosslinking density feature a more porous structure, which accelerates both swelling and deswelling processes by enhancing the diffusion of water into and out of the hydrogel matrix [39].

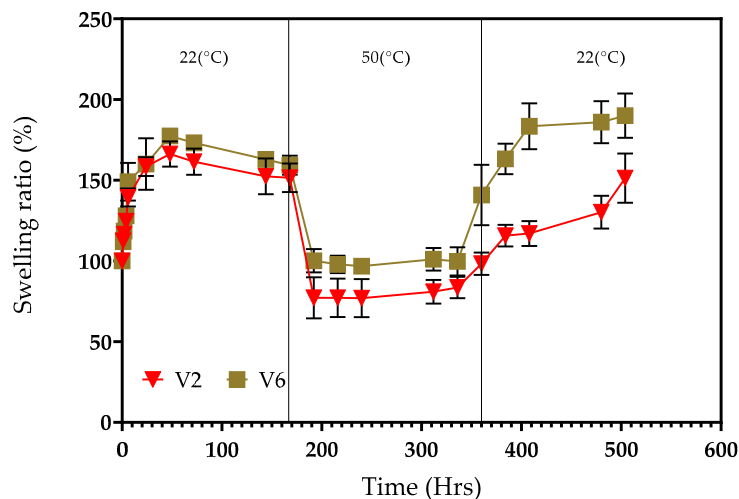


**Figure 8.** The swelling ratio of samples V2 and V6 was conducted at ambient temperature ( $\sim 22^\circ\text{C}$ ) and  $50^\circ\text{C}$ . ( $\blacktriangledown$ ) P(NVCL90-DEGDA10) and ( $\blacksquare$ ) P(NVCL70-DEGDA10-VAc20).

### 3.6. Gel Fraction Measurement

Gel fraction measurement acts as a qualitative measure to assess the effectiveness of network formation within the 3D printed sample. It indicates the extent of crosslinking that takes place among the polymer chains within the 3D printed sample. A higher percentage of gel fraction suggests a greater density of crosslinks formed. As a result, the swelling capacity of the 3D printed sample is reduced due to the increased network density [40]. The gel fraction percentages for all samples are displayed in Figure 9. The results indicated that the gel fraction percentage was in the range of 93% to 26%. Sample V1, resulted in a low gel fraction percentage, which is in line with the swelling results achieved. The gel fraction percentage increased dramatically by increasing the concentration of DEGDA to 10 wt%; sample V2 maintained a gel fraction measurement of 79%. Again, there was an increase in gel fraction to 92% for samples containing 40 wt% DEGDA. Therefore, it was observed that the addition of a high level of crosslinker, DEGDA, led to a higher density of formed crosslinks, which, in turn, led to a reduction in the swelling capability, as evident from Section 3.5.

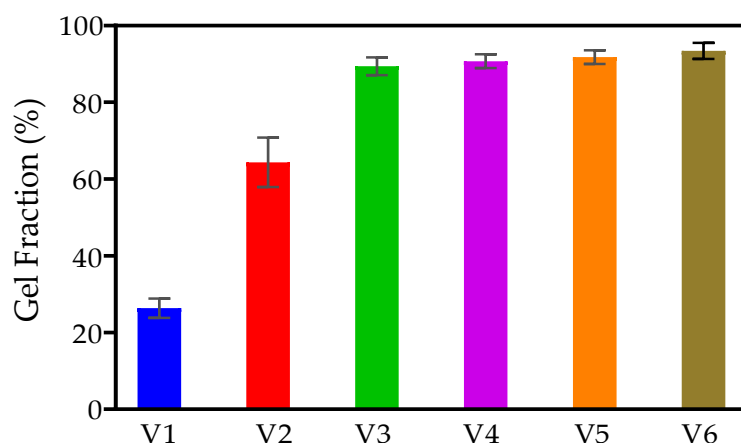


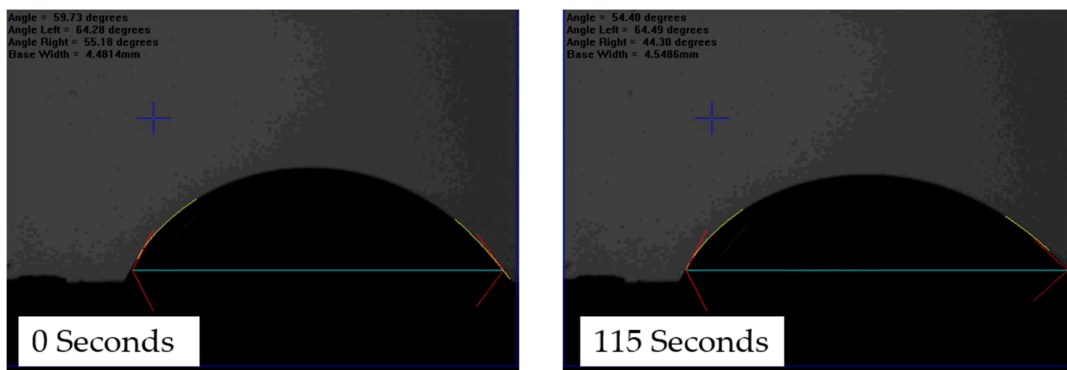
**Figure 9.** The comparison of gel fraction percentage for samples V1, V2, V3, V4, V5, and V6.

### 3.7. Goniometry

Goniometry is a technique used to measure contact angles, which is the angle formed at the interface between a liquid droplet and a solid surface. The contact angle measurement provides the hydrophilicity or hydrophobicity of the 3D print surface. A contact angle closer to  $0^\circ$  indicates a higher level of hydrophilicity, meaning the material has a strong

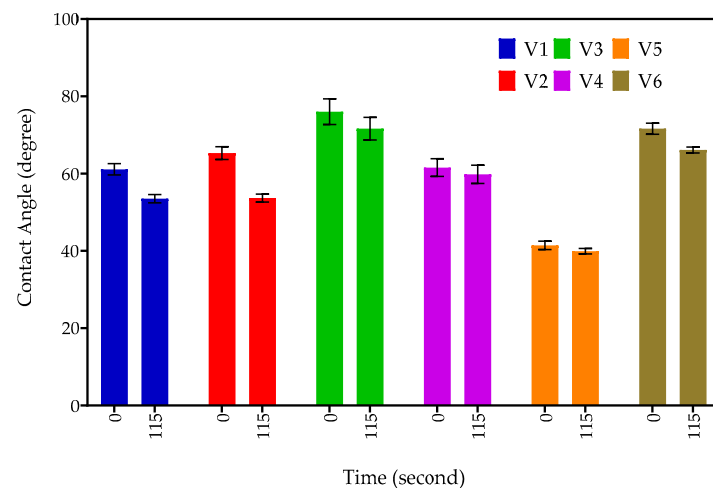
affinity to water. Hydrophilic materials typically have contact angles up to  $90^\circ$ . On the other hand, materials with contact angles greater than  $90^\circ$  are considered hydrophobic, as they exhibit reduced affinity for water. When the contact angle on a surface exceeds  $150^\circ$ , called superhydrophobic, indicating that a liquid droplet interacts with the surface without causing substantial wetting [24].

Figure 10 presents the contact angle measurements for sample V1 at two time points: 0 s and 115 s. At the initial measurement (0 s), the contact angle for V1 was recorded at  $61.10^\circ$ , which subsequently decreased to  $53.52^\circ$  after 115 s.



**Figure 10.** Indication of the contact angle obtained at 0 s and 115 s of sample V1.

Sample V2 exhibited an average contact angle of  $65.31^\circ$  at 0 s, dispersing into a drop, which then decreased to an average contact angle of  $53.68^\circ$  after 115 s. This indicates that the 3D printed sample is a hydrophilic material, therefore having the ability to absorb water. Swelling behaviour is crucial in 4D printing as it enables shape-changing capabilities. By increasing the concentration of the DEGDA to 40 wt%, sample V5 displayed an average contact angle of  $44.89^\circ$  at 0 s, spreading into a drop with a mean contact angle of  $39.91^\circ$  at 115 s. Increasing the concentration of crosslinker in the 3D printed sample showed a reduction in the contact angle. However, V6, incorporated with 20 wt% VAc, resulted in a reduction in the mean contact angle in comparison to samples containing only the DEGDA crosslinker. Sample V6 displayed a mean contact angle of  $71.62^\circ$  at 0 s, which decreased to  $66.12^\circ$  at 115 s. Overall, goniometry results indicated that the higher the concentration of crosslinker present in the 3D printed sample, the sample demonstrated a much stronger affinity to water. This was evident between samples V3, V4, and V5. Sample V6 illustrated the addition of a comonomer has minimal effect on the mean contact angle. The mean contact angles of the samples are outlined in Figure 11.



**Figure 11.** At 0 s and 115 s, the contact angle of samples V1, V2, V3, V4, V5, and V6.

#### 4. Conclusions

The primary goal of this study is to enhance the understanding of the synthesis and characterisation of NVCL-co-DEGDA resin for 4D printing purposes. This study outlines the process of the fabrication of NVCL-co-DEGDA resin for 4D printing using a Form 2 SLA 3D printer. The samples were characterised by DSC, pulsatile swelling studies, Goniometry, and gel fraction measurements. It was found that the  $T_g$  of the 3D printed samples showed an inverse relationship between the  $T_g$  values and the concentration of crosslinker. The higher the amount of DEGDA present, the lower the  $T_g$ . Pulsatile swelling studies indicated that an increased concentration of DEGDA in the 3D printed samples correlated with a prolonged time required to reach the maximum swelling ratio. Gel fraction measurement showed that with the addition of a high level of DEGDA within the 3D printed sample, a higher density of crosslinks formed, which led to a reduction in the swelling capability. The goniometry results indicated that the higher the concentration of crosslinker present in the 3D printed sample, the sample demonstrated a much stronger affinity to water.

Moving forward, the focus will be to demonstrate this NVCL-co-DEGDA resin presented in this paper for the fabrication of 4D printed stents with controlled swelling behaviour. The integration of responsive materials into medical devices holds a promising future for patient-specific treatments.

**Author Contributions:** E.H. and L.M.G. conceived and designed the experiments and were supported by B.S.H.T., S.Z. and G.K.; E.H. performed the experiments; E.H. analysed the data; E.H. wrote the paper; S.Z., M.A., B.S.H.T., G.K., D.M.C. and L.M.G. reviewed the paper. All authors have read and agreed to the published version of the manuscript.

**Funding:** This research was funded by AMBER, SFI Centre for Advanced Materials and BioEngineering Research.

**Institutional Review Board Statement:** Not applicable.

**Data Availability Statement:** Data are contained within the article.

**Acknowledgments:** The authors are grateful to AMBER, SFI Centre for Advanced Materials and BioEngineering Research, for their research support and purchasing of materials for this study.

**Conflicts of Interest:** The authors declare no conflicts of interest. The funders had no role in the design of the study; in the collection, analyses, or interpretation of data; in the writing of the manuscript; or in the decision to publish the results.

#### References

1. Karkun, M.S.; Dharmalingam, S. 3D Printing Technology in Aerospace Industry – A Review. *Int. J. Aviat. Aeronaut. Aerosp.* **2022**, *9*, 4. [[CrossRef](#)]
2. Elakkad, A.S. 3D Technology in the Automotive Industry. *Int. J. Eng. Res.* **2019**, *8*, 248–251. [[CrossRef](#)]
3. Aimar, A.; Palermo, A.; Innocenti, B. The Role of 3D Printing in Medical Applications: A State of the Art. *J. Health Eng.* **2019**, *2019*, 5340616. [[CrossRef](#)]
4. Fan, D.; Li, Y.; Wang, X.; Zhu, T.; Wang, Q.; Cai, H.; Li, W.; Tian, Y.; Liu, Z. Progressive 3D Printing Technology and Its Application in Medical Materials. *Front. Pharmacol.* **2020**, *11*, 122. [[CrossRef](#)]
5. Shahrubudin, N.; Lee, T.C.; Ramlan, R. An overview on 3D printing technology: Technological, materials, and applications. *Procedia Manuf.* **2019**, *35*, 1286–1296. [[CrossRef](#)]
6. Reddy, S. *Smart Materials for 4D Printing: A Review on Developments, Challenges and Applications*; Springer: Singapore, 2022.
7. Ahmed, A.; Arya, S.; Gupta, V.; Furukawa, H.; Khosl, A.A. 4D printing: Fundamentals, materials applications and challenges. *Polymer* **2021**, *228*, 123926. [[CrossRef](#)]
8. Momeni, F.; Hassani, S.M.M.; Liu, X.; Ni, J. A review of 4D printing. *Mater. Des.* **2017**, *122*, 42–79. [[CrossRef](#)]
9. Kafle, A.; Luis, E.; Silwal, R.; Pan, H.M.; Shrestha, P.L.; Bastola, A.K. 3d/4d printing of polymers: Fused deposition modelling (FDM), selective laser sintering (SLS), and stereolithography (SLA). *Polymers* **2021**, *13*, 3101. [[CrossRef](#)]
10. Hu, G.; Cao, Z.; Hopkins, M.; Hayes, C.; Daly, M.; Zhou, H.; Devine, D.M. Optimizing the hardness of SLA printed objects by using the neural network and genetic algorithm. *Procedia Manuf.* **2019**, *38*, 117–124. [[CrossRef](#)]

11. Aldawood, F.K. A Comprehensive Review of 4D Printing: State of the Arts, Opportunities, and Challenges. *Actuators* **2023**, *12*, 101. [[CrossRef](#)]
12. Kök, M.; Qader, İ.N.; Dağdelen, F.; Aydoğdu, Y. A Review of Smart Materials: Researches and Applications. *El-Cezeri Fen Mühendislik Derg.* **2019**, *2019*, 755–788.
13. Haleem, A.; Javaid, M.; Singh, R.P.; Suman, R. Significant roles of 4D printing using smart materials in the field of manufacturing. *Adv. Ind. Eng. Polym. Res.* **2021**, *4*, 301–311. [[CrossRef](#)]
14. Imrie, P.; Jin, J. Polymer 4D printing: Advanced shape-change and beyond. *J. Polym. Sci.* **2022**, *60*, 149–174. [[CrossRef](#)]
15. Gazzaniga, A.; Foppoli, A.; Cerea, M.; Palugan, L.; Cirilli, M.; Moutaharrik, S.; Melocchi, A.; Maroni, A. International Journal of Pharmaceutics: X Towards 4D printing in pharmaceutics. *Int. J. Pharm.* **2023**, *5*, 100171.
16. Sahafnejad-Mohammadi, I.; Karamimoghadam, M.; Zolfagharian, A.; Akrami, M.; Bodaghi, M. 4D printing technology in medical engineering: A narrative review. *J. Braz. Soc. Mech. Sci. Eng.* **2022**, *44*, 233. [[CrossRef](#)]
17. Manaia, J.P.; Cerejo, F.; Duarte, J. Revolutionising textile manufacturing: A comprehensive review on 3D and 4D printing technologies. *Fash. Text.* **2023**, *10*, 20. [[CrossRef](#)]
18. Nkomo, N.Z. A Review of 4D Printing Technology and Future Trends. In Proceedings of the Eleventh South African Conference on Computational and Applied Mechanics, Vanderbijlpark, South Africa, 17–19 September 2018.
19. Cortez-Lemus, N.A.; Licea-Claverie, A. Poly(N-vinylcaprolactam), a comprehensive review on a thermoresponsive polymer becoming popular. *Prog. Polym. Sci.* **2016**, *53*, 1–51. [[CrossRef](#)]
20. Killion, J.A.; Kehoe, S.; Geever, L.M.; Devine, D.M.; Sheehan, E.; Boyd, D.; Higginbotham, C.L. Hydrogel/bioactive glass composites for bone regeneration applications: Synthesis and characterisation. *Mater. Sci. Eng. C* **2013**, *33*, 4203–4212. [[CrossRef](#)]
21. Xu, R. Light scattering: A review of particle characterization applications. *Particuology* **2015**, *18*, 11–21. [[CrossRef](#)]
22. Bastiancich, C.; Danhier, P.; Pr at, V. Anticancer drug-loaded hydrogels as drug delivery systems for the local treatment of glioblastoma. *J. Control. Release* **2016**, *243*, 29–42. [[CrossRef](#)]
23. Arefin, A.M.E.; Khatri, N.R.; Kulkarni, N.; Egan, P.F. Polymer 3D printing review: Materials, process, and design strategies for medical applications. *Polymers* **2021**, *13*, 1499. [[CrossRef](#)]
24. Zhuo, S.; Geever, L.M.; Halligan, E.; Tie, B.S.H.; Breheny, C. A Development of New Material for 4D Printing and the Material Properties Comparison between the Conventional and Stereolithography Polymerised NVCL Hydrogels. *J. Funct. Biomater.* **2022**, *13*, 262. [[CrossRef](#)]
25. Choong, Y.Y.C.; Maleksaeedi, S.; Eng, H.; Wei, J.; Su, P.-C. 4D printing of high performance shape memory polymer using stereolithography. *Mater. Des.* **2017**, *126*, 219–225. [[CrossRef](#)]
26. Karagianni, A.; Kachrimanis, K.; Nikolakakis, I. Co-amorphous solid dispersions for solubility and absorption improvement of drugs: Composition, preparation, characterization and formulations for oral delivery. *Pharmaceutics* **2018**, *10*, 98. [[CrossRef](#)]
27. Moraes, R.M.; Carvalho, L.T.; Alves, G.M.; Medeiros, S.F.; Bourgeat-Lami, E.; Santos, A.M. Synthesis and Self-Assembly of Poly(N-Vinylcaprolactam)-*b*-Poly( $\epsilon$ -Caprolactone) Block Copolymers via the Combination of RAFT/MADIX and Ring-Opening Polymerizations. *Polymers* **2020**, *12*, 1252. [[CrossRef](#)]
28. Usanmaz, A.;  zdemir, T.; Polat,  . Solid state polymerization of N-vinylcaprolactam via gamma irradiation and characterization. *J. Macromol. Sci. Part A* **2009**, *46*, 597–606. [[CrossRef](#)]
29. Yang, S.B.; Karim, M.R.; Lee, J.; Yeum, J.H.; Yeasmin, S. Alkaline Treatment Variables to Characterize Poly(Vinyl Alcohol)/Poly(Vinyl Butyral/Vinyl Alcohol) Blend Films. *Polymers* **2022**, *14*, 3916. [[CrossRef](#)]
30. Chowdhury, J.; Anirudh, P.V.; Karunakaran, C.; Rajmohan, V.; Mathew, A.T.; Koziol, K.; Alsanie, W.F.; Kannan, C.; Balan, A.S.S.; Thakur, V.K. 4D printing of smart polymer nanocomposites: Integrating graphene and acrylate based shape memory polymers. *Polymers* **2021**, *13*, 3660. [[CrossRef](#)]
31. Kirsh, Y.; Yanul, N.; Kalnins, K. Structural transformations and water associate interactions in poly-N-vinylcaprolactam–water system. *Eur. Polym. J.* **1999**, *35*, 305–316. [[CrossRef](#)]
32. Meng, W.; Gao, L.; Venkatesan, J.K.; Wang, G.; Madry, H.; Cucchiari, M. Translational applications of photopolymerizable hydrogels for cartilage repair. *J. Exp. Orthop.* **2019**, *6*, 47. [[CrossRef](#)] [[PubMed](#)]
33. Halligan, S.C.; Dalton, M.B.; Murray, K.A.; Dong, Y.; Wang, W.; Lyons, J.G.; Geever, L.M. Synthesis, characterisation and phase transition behaviour of temperature-responsive physically crosslinked poly (N-vinylcaprolactam) based polymers for biomedical applications. *Mater. Sci. Eng. C* **2017**, *79*, 130–139. [[CrossRef](#)]
34. Parhi, R. Cross-Linked Hydrogel for Pharmaceutical Applications: A Review. *Tabriz Univ. Med. Sci.* **2017**, *7*, 515–530. [[CrossRef](#)]
35. Heck, T.; Faccio, G.; Richter, M.; Th ny-Meyer, L. Enzyme-catalyzed protein crosslinking. *Appl. Microbiol. Biotechnol.* **2013**, *97*, 461–475. [[CrossRef](#)]
36. Cozens, E.J.; Roohpour, N.; Gautrot, J.E. Comparative adhesion of chemically and physically crosslinked poly(acrylic acid)-based hydrogels to soft tissues. *Eur. Polym. J.* **2021**, *146*, 110250. [[CrossRef](#)]
37. Singh, A.K.; Itkor, P. State-of-the-Art Insights and Potential Applications of Cellulose-Based Hydrogels in Food Packaging: Advances. *Gels* **2023**, *9*, 433. [[CrossRef](#)]
38. Maitra, J.; Shukla, V.K. Cross-linking in Hydrogels—A Review. *Am. J. Polym. Sci.* **2014**, *4*, 25–31.

39. Ngadaonye, J.I.; Cloonan, M.O.; Geever, L.M.; Higginbotham, C.L. Synthesis and characterisation of thermo-sensitive terpolymer hydrogels for drug delivery applications. *J. Polym. Res.* **2011**, *18*, 2307–2324. [[CrossRef](#)]
40. Barleany, D.R.; Ananta, C.V.; Maulina, F.; Rochmat, A.; Alwan, H.; Erizal, E. Controlled release of metformin hydrogen chloride from stimuli-responsive hydrogel based on poly(N-Isopropylacrylamide)/Chitosan/Polyvinyl alcohol composite. *Int. J. Technol.* **2020**, *11*, 511–521. [[CrossRef](#)]

**Disclaimer/Publisher’s Note:** The statements, opinions and data contained in all publications are solely those of the individual author(s) and contributor(s) and not of MDPI and/or the editor(s). MDPI and/or the editor(s) disclaim responsibility for any injury to people or property resulting from any ideas, methods, instructions or products referred to in the content.